Title

Defluorination Mechanisms and Real-Time Dynamics of Per- and Polyfluoroalkyl Substances on Electrified Surfaces

Journal

Environmental Science & Technology Letters, 12(2)

ISSN

2328-8930

Authors

Sharkas, Kamal
Wong, Bryan M

Publication Date

2025-02-11

DOI

10.1021/acs.estlett.4c01130

Defluorination Mechanisms and Real-Time Dynamics of Per- and Polyfluoroalkyl Substances on Electrified Surfaces

Kamal Sharkas and Bryan M. Wong*

Department of Chemistry, Department of Physics & Astronomy, and Materials Science & Engineering Program, University of California-Riverside, Riverside, California 92521, United States

E-mail: bryan.wong@ucr.edu,Website:http://www.bmwong-group.com

Abstract

Per- and polyfluoroalkyl substances (PFAS) are persistent environmental contaminants found in groundwater sources and a wide variety of consumer products. In recent years, electrochemical approaches for the degradation of these harmful contaminants have garnered significant attention due to their efficiency and chemical-free modular nature. However, these electrochemical processes occur in open, highly non-equilibrium systems, and a detailed understanding of PFAS degradation mechanisms in these promising technologies is still in its infancy. To shed mechanistic insight into these complex processes, we present the first constant-electrode potential (CEP) quantum calculations of PFAS degradation on electrified surfaces. These advanced CEP calculations provide new mechanistic details on the intricate electronic processes that occur during PFAS degradation in the presence of an electrochemical bias, which cannot be gleaned from conventional DFT calculations. We complement our CEP calculations with large-scale *ab initio* molecular dynamics simulations in the presence of

an electrochemical bias to provide timescales for PFAS degradation on electrified surfaces. Taken together, our CEP-based quantum calculations provide critical reaction mechanisms for PFAS degradation in open electrochemical systems, which can be used for pre-screening candidate material surfaces and optimal electrochemical conditions for remediating PFAS and other environmental contaminants.

Keywords: PFAS, constant electrode potential, electrified surfaces, defluorination, density functional theory

Synopsis: We present the first constant-electrode potential quantum calculations to understand PFAS degradation mechanisms on electrified surfaces.

1. Introduction

Per- and polyfluoroalkyl substances (PFAS) are synthetic compounds with strong C–F bonds that endow them with exceptional chemical and thermal stability. Because of this intrinsic stability, PFAS have been used in a variety of consumer products, such as packaging materials, non-stick cookware, stain-resistant fabrics, surfactants, and firefighting foams.[1–4] Due to their widespread use, PFAS contaminants have now been detected in soil/water sources worldwide and can bioaccumulate in the food chain. The persistence of these environmental pollutants is particularly concerning, since chronic exposure to even low concentration levels has been associated with adverse health effects. Because of their environmental persistance and toxicity, finding efficient approaches to eliminating these contaminants is essential.

Among the various oxidation/reduction processes[5–11] used for PFAS remediation, electrochemical approaches have garnered particular attention due to their efficiency and chemical-free modular nature.[12] In these electrochemical processes, an external bias voltage is applied to an electrolytic solution of PFAS contaminants, which facilitates electron transfer and subsequent PFAS degradation on the electrified surface of the electrode. More specifically, at the electrode-electrolyte interface, PFAS molecules interact with both the electrode surface and the solvent. This interface (by definition) is an open, non-equilibrium thermodynamic system

that exchanges matter and energy with its surroundings and facilitates electrochemical reactions driven by the potential difference between the electrodes and the electrolyte. Due to the inherent complexity of these electrochemical processes, a detailed understanding of PFAS degradation mechanisms in these complex environments is scarce and still in its infancy.[13–16] For example, the choice of electrode material, electrolyte composition/concentration, temperature, and external bias are all experimental conditions that can be modified, but it is not obvious which combinations of these parameters are optimal for PFAS degradation. Moreover, since the entire electrochemical system is under an external bias, conventional density functional theory (DFT) in its standard formulation (discussed further below) cannot be used, since the system is open and driven far from equilibrium.[17] To shed mechanistic insight into these electrochemically-induced processes, we present the first constant-electrode potential (CEP) quantum calculations of PFAS degradation on electrified surfaces. The application of CEP quantum calculations to electrochemically-induced PFAS degradation is particularly novel since traditional DFT methods are *inherently constrained to a fixed number of electrons* and cannot capture realistic electrochemical conditions where there is a facile exchange of electrons with the electrode. Our CEP calculations go beyond this limitation by modifying the conventional DFT formalism to allow electrons to be freely supplied/removed from the system (via the electrode potential), which accurately simulates a realistic electrochemical interface. This approach allows us to simulate the true grand-canonical thermodynamic ensemble of electrons, capturing the critical Fermi-level fluctuations that govern the complex reactivity in these electrochemical systems. We describe our approaches for simulating these complex, non-equilibrium processes, followed by a variety of analyses and real-time dynamics that explain the underlying mechanisms of the electrochemically-induced degradation process. Finally, we conclude with a discussion and summary of our results, with additional perspectives on future applications of our CEP-based techniques that can have a broad impact on electrochemical degradation of PFAS.

2. Methods and Materials

We investigated PFAS degradation reactions in the presence of a constant-electrode potential (CEP)[18] using a locally modified Vienna Ab initio Simulation Package (VASP)[19,20] code with the VASPsol[21,22] implicit solvation model. In the CEP model, density functional theory[23,24] (DFT) calculations with *varying numbers of electrons* are iteratively carried out for the entire chemical system in the presence of an implicit electrolyte. It is worth emphasizing that these CEP calculations go beyond the conventional canonical DFT formalism since the entire system is open (i.e., a grand canonical thermodynamic system), and the total number of electrons in the system is iteratively adjusted until the Fermi level, E_F, converges to the applied electrode potential, U (in volts). A solution for the CEP system is obtained when the following expression is self-consistently satisfied:

$$U = \frac{-E_F - \phi_{\mathrm{SHE}}}{e}, \tag{1}$$

where $\phi_{\mathrm{SHE}} = 4.6$ eV is the work function of the standard hydrogen electrode (SHE) as calculated with the Perdew-Burke-Ernzerhof (PBE)[25] functional in the VASPsol model, and e is the elementary charge. We used a 0.01 eV convergence criterion for the electrolyte-referenced Fermi level to solve Eq. (1) self-consistently.

We investigated a protonated PFOA ($C_7F_{15}COOH$) molecule adsorbed on an electrode surface, which was modeled with a 4-layer, 5×5 Cu(111) slab. The Cu(111) surface was specifically chosen for our studies since Cu is one of the most widely used transition metal catalysts (due to its abundance and low cost), and the Cu(111) surface is one of the most well-studied metal surfaces in both experimental and theoretical studies.[26] We also carried out additional calculations with larger slabs and verified that the 5×5 Cu(111) slab used in our work was sufficiently large enough to give accurate results. The PFOA molecule was adsorbed on the Cu(111) surface in the lowest-energy "flat" configuration[27] where the plane of the carbon backbone is parallel to the surface. To avoid spurious interactions between the adjacent

chemical species in repeated supercells, a ∼25 Å vacuum spacing was used along the surface normal. In the remainder of this work, we denote this supercell as PFOA/Cu(111), which has 1,850 valence electrons. Both static (i.e., single point/structural relaxation) and molecular dynamics[28] DFT simulations were carried out with periodic boundary conditions under a fixed electrode potential with projector augmented-wave (PAW) pseudopotentials.[29,30] We used a Debye length of 3.0 Å in the VASPSol package, which corresponds to a bulk electrolyte with a 1 M concentration of monovalent cations and anions and a relative permittivity of the solvent of 80 for water at ambient conditions. The dispersion-corrected PBE-D3[31] functional with a 520 eV cutoff energy was used for the plane-wave expansion. The optimized structure of PFOA/Cu(111) is illustrated in Fig. S1 of the Supporting Information (SI). The Brillouin zone was sampled with a 2×2×1 Monkhorst–Pack mesh; the electronic energy and forces were converged to within 1×10^{-6} eV and 0.02 eV/Å, respectively. During the simulations, the bottom layer of the Cu electrode was held fixed at the optimized bulk structure. The *ab initio* molecular dynamics (AIMD) simulations were performed at 300 K with the Nosé-Hover thermostat.[32]

3. Results and Discussion

Using the optimized supercell geometries depicted in Fig. S1 in the SI, we carried out CEP ionic-relaxation and AIMD calculations for several values of the applied bias to study PFOA degradation dynamics on the electrified electrode surfaces.

3.1 PFAS Degradation Mechanisms on Electrified Electrode Surfaces

We explored a wide range of applied anodic(+)/cathodic(-) voltages (spanning from -3 to +3 V) with respect to the SHE, and Fig. S2 in the SI shows the optimized structure of the PFOA/Cu(111) supercell from these CEP ionic-relaxation calculations. Fig. 1(a)

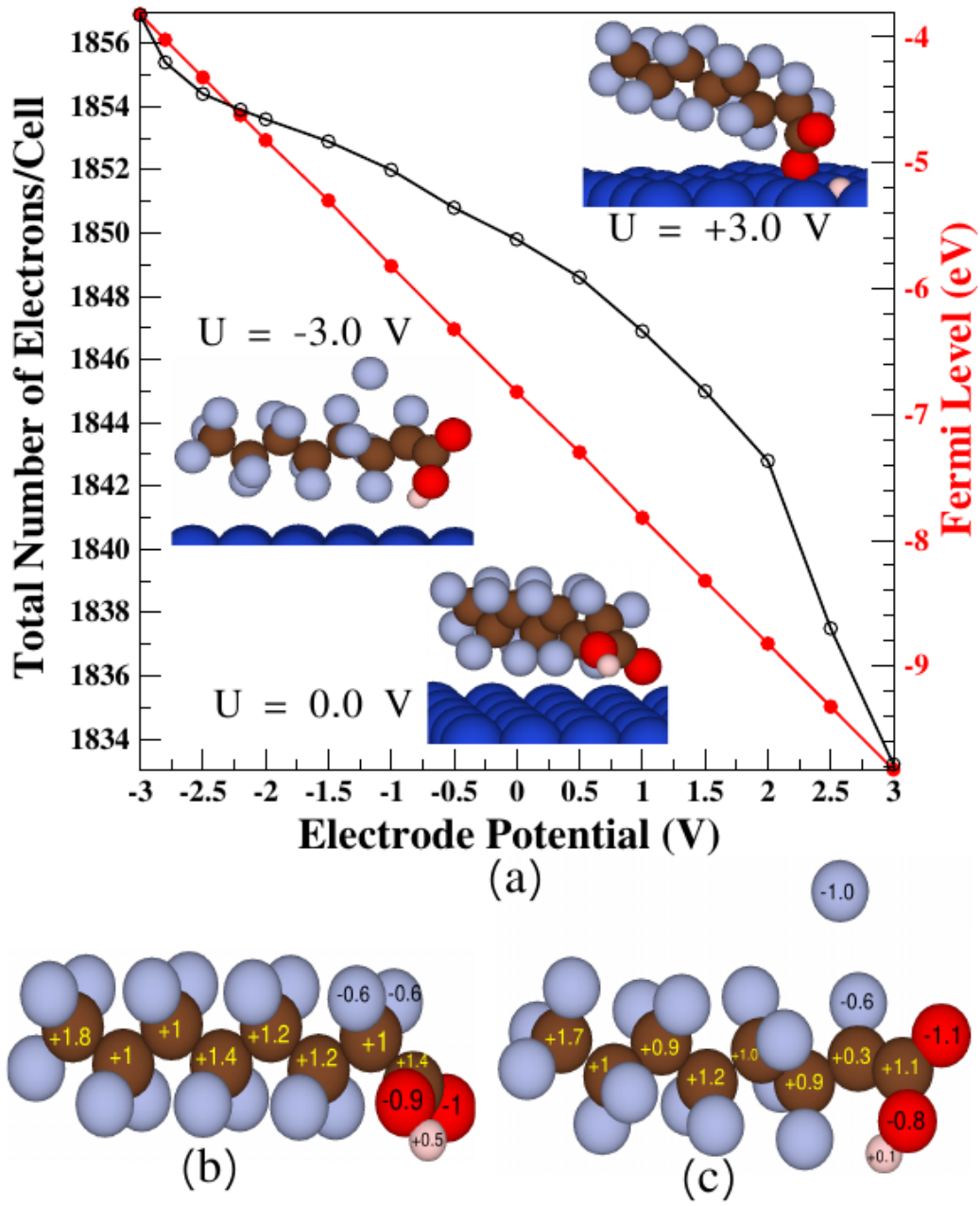

Figure 1: (a) Total number of electrons, N_e (left vertical axis; hollow circles), and Fermi level, E_F (right vertical axis; solid circles), vs. the applied electrode potential. The three structures in panel (a) depict the optimized geometries of the PFOA/Cu(111) supercell obtained from the constant-electrode potential ionic-relaxation calculations at an applied bias of -3.0, 0.0, and +3.0 V. (b) and (c) Bader charge analysis for PFOA in the structurally optimized PFOA/Cu(111) supercell at an applied bias of 0.0 and -3.0 V, respectively. The PFOA geometries are identical to those shown inside panel (a). The numbers on the atoms show their Bader net atomic charges (in units of e). To simplify the visualization, the charges on the backbone F (gray) atoms ($\sim$-0.6 e) are not displayed since they do not differ significantly between panels (b) and (c). The atoms are denoted by the following coloring scheme: H (white), C (brown), O (red), F (gray), and Cu (blue).

plots the converged total number of electrons, N_e (left vertical axis; hollow circles), and Fermi level, E_F (right vertical axis; solid circles), for the CEP ionic-relaxation calculations for PFOA/Cu(111) as a function of the applied electrode potential. At 0.0 V, the CEP-optimized geometry (illustrated on the lowest snapshot of Fig.1 (a)) shows a minor structural deviation from the initial PFOA/Cu(111) geometry (see panels Figs. S1(a) and (b) in the SI) However, when +1.0 V is applied, the plane of the carboxyl ($-$COOH) group rotates and moves the carbonyl oxygen/hydroxyl group closer to/farther from the surface plane (see Fig. S2(b) in the SI). This positive voltage effectively reduces N_e by almost 3 electrons to 1846.9 e^- and shifts E_F downward to -7.8 eV. At a potential of +2.0 V, the carbonyl oxygen forms a bond with the copper surface, and the hydroxyl group dissociates. The liberated hydrogen atom subsequently binds to an on-top site on the Cu(111) surface (see Fig. S2(d) in the SI). Further increasing the potential to +3.0 V effectively removes nearly 17 electrons from the neutral reference system and triggers the migration of the hydrogen atom to a hollow site on the Cu(111) surface (see Fig. S2(f) in the SI). Apart from this deprotonation reaction, no additional degradation pathways for PFOA were identified at potentials up to +3.0 V. Increasing the potential beyond this limit results in extremely difficult convergence of the CEP calculations since the depletion of electrons creates a large positive charge in the periodic cell, which is unphysical. Our findings are also consistent with several experimental studies showing that oxidation processes at positive applied voltages can be less efficient than reduction processes (which occur at a negative applied bias) for degradation of PFAS.[13–16]

Turning our attention to negative voltages, Figs. S2(c, e, and g) in the SI show that the carboxyl group plane in PFOA rotates in the opposite direction compared to the geometries obtained under positive voltages. As shown in Fig. 1(a), negative biases result in more electrons introduced into the PFOA/Cu(111) supercell (compared to the zero-bias state with $N_e = 1850.0\ e^-$), which accelerates PFOA defluorination via excess electrons in this reductive process. This phenomenon also manifests itself in the increasing Fermi level as the voltage is decreased, as shown in Fig. 1(a). We observed no significant structural changes in

PFOA for voltages more positive than -3.0 V; however, at this critical value of the bias, the CEP ionic-relaxation simulations show the dissociation of a C−F bond located at the C2 carbon (carbon-atom numberings in this work, i.e., C2 or C6, are denoted by their distance from the carboxyl head group); see structure on the middle left side of Fig. 1(a). This agrees well with previous experimental findings that indicate C–F bond cleavage occurs at potentials close to -3.0 V.[11,33,34]

To further understand the effects of applying a negative potential to the system, we carried out a Bader charge analysis[35,36] for the PFOA/Cu(111) system at 0.0 (N_e = 1849.8 e^-) and -3.0 V (N_e = 1856.9 e^-). This analysis reveals that approximately 68% (∼4.8 e^-) of the 7.1 additional electrons in the cell at -3.0 V are retained within the Cu(111) surface slab, while about 32% (∼2.3 e^-) are transferred to PFOA. Figs. 1(b) and (c) show the results of the Bader charge analysis for the PFOA/Cu(111) system at applied electrode potentials of 0.0 and -3.0 V, respectively. The numerical labels on each atom denote their Bader net atomic charges, which are determined by the difference between the number of valence electrons and the Bader population associated with that atom. At 0.0 V, the nearly neutral PFOA consists of 15 negatively charged F atoms (-0.6 e) on the carbon backbone. In contrast, the carbon atoms have charges ranging from +1 to +1.8 e and are connected to a carboxyl group with negatively-charged oxygen atoms and a +0.5 e-charged hydrogen atom. This analysis reflects the well-known partial ionic character of the C−F bond where the high electronegativity of fluorine creates a partial positive and negative charge on C and F, respectively. Upon application of a negative voltage of -3.0 V, dramatic changes occur within the PFOA molecule. The positive charge on the H atom decreases to +0.1 e as it gets closer to the surface. Moreover, the C2 carbon atom experiences a significant decrease to +0.3 e, and the external voltage leads to cleavage of the C2–F bond. As a result, a negatively charged fluoride ion (F^-) is released from the molecule and migrates into the surrounding electrolyte solution.

To understand the electronic mechanisms of the C–F dissociation process in the presence

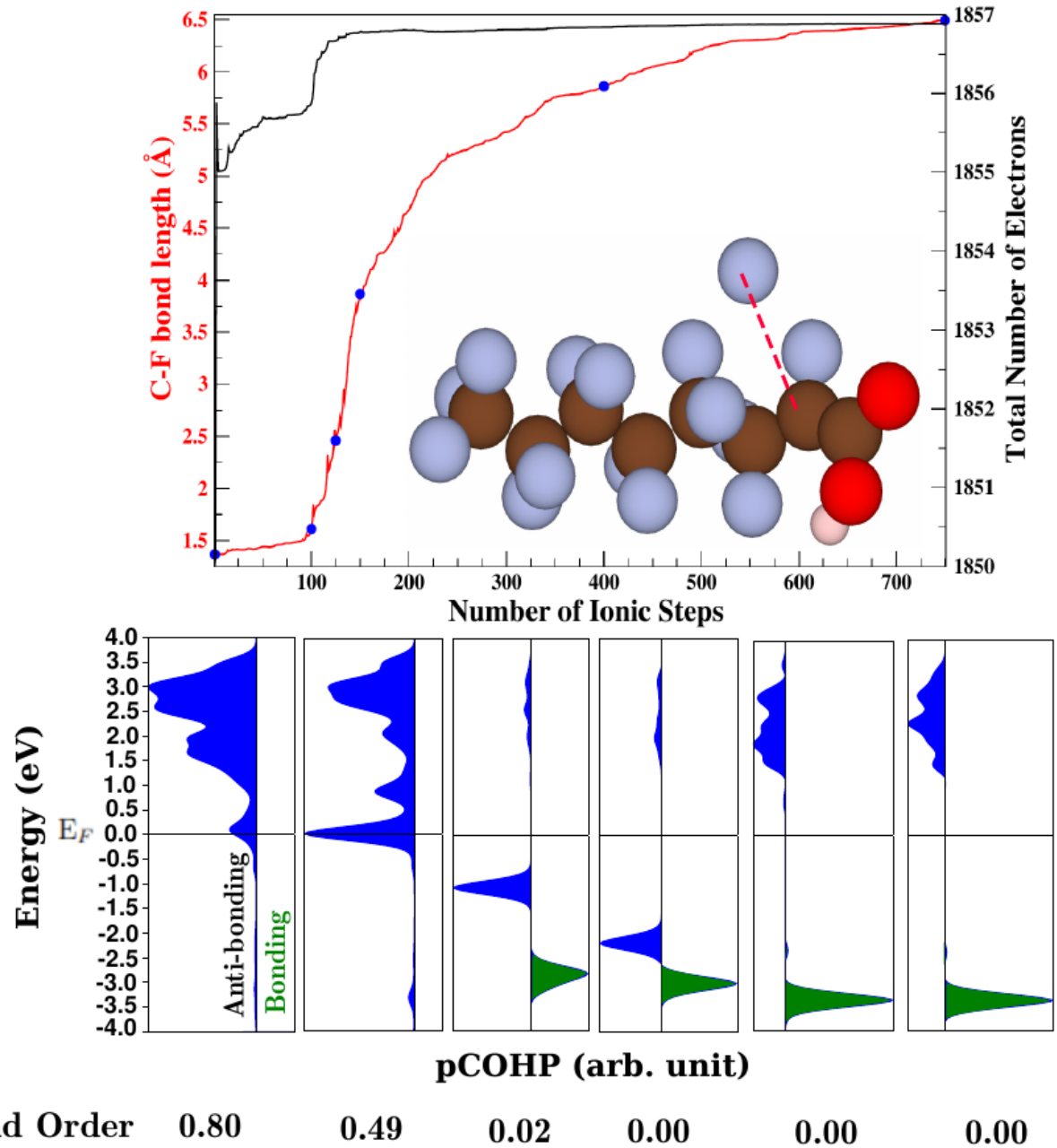

Figure 2: (Upper panel) Evolution of the C2–F bond, indicated by the dashed red line on the PFOA structure; C–F bond length (left vertical axis) as a function of the number ionic steps during the CEP ionic relaxation calculation at -3.0 V. The black curve plots the total number of electrons (right vertical axis) in the PFOA/Cu(111) supercell during the same simulation. (Lower panels) Projected crystal orbital Hamilton population (pCOHP) bonding analysis for the C2–F bond at six different lengths (solid blue circles on the upper red curve). The left (blue)/right (green) sides of the COHP curves denote the anti-bonding/bonding distributions, respectively; the bond order of the C2–F bond is reported at the bottom of the figure.

of an applied bias, we used the Crystal Orbital Hamilton Population (COHP) analysis in the LOBSTER[37] software package. In the COHP formalism, bonding, non-bonding, and antibonding interactions are identified for pairs of atoms in a given structure, and the integrated value of the crystal orbital bond index (ICOBI) equals the chemical bond order. The upper panel of Fig. 2 depicts the evolution of the C2–F bond length (R_{C-F}, left vertical axis) and the total number of electrons (right vertical axis) throughout the 750 ionic steps of the CEP ionic-relaxation calculation at -3.0 V. The lower panels of Fig. 2 report the projected crystal orbital Hamilton population (pCOHP) bonding analysis of the C2–F bond at six different lengths (denoted as solid blue circles on the bond length vs. ionic steps curve) as a function of energy. For each bond length, the value of the chemical bond order is reported under the associated pCOHP curve in which the Fermi level (E_F) lies at zero eV, and the left (blue)/right (green) sides are the anti-bonding/bonding distributions, respectively. At the first ionic step ($R_{C-F} = 1.367$ Å and $N_e = 1850.0\ e^-$), the bond order of 0.80 indicates a weaker bond compared to a pure single bond with an order of 1.0. This suggests that the bond is less stable and more susceptible to breaking under the applied bias as the ionic relaxation simulation progresses. In the associated pCOHP curve, the presence of C−F antibonding states near the Fermi level signifies electronic instability within the system. At the 100th ionic step ($R_{C-F} = 1.612$ Å and $N_e = 1855.9\ e^-$), the bond order has significantly decreased to 0.49, indicating a further weakening of the bond. The pCOHP plot shows that this bond weakening is accompanied by an increase in antibonding interactions below the Fermi level. While the antibonding states vanish at the Fermi level by the 125th ionic step ($R_{C-F} = 2.460$ Å and $N_e = 1856.7\ e^-$), the electronic instability persists. This persistence is attributed to the presence of populated antibonding states, which gradually diminish as the simulation progresses towards the 150th step ($R_{C-F} = 3.868$ Å and $N_e = 1856.8\ e^-$). At this point, the bond order reaches zero, signifying a complete bond dissociation. Elongation of the C2–F bond during the ionic relaxation process leads to the complete depletion of occupied antibonding states. By the final ionic step ($R_{C-F} = 6.494$ Å and $N_e = 1856.9\ e^-$), the

Fermi level in the pCOHP curve resides within a gap between the bonding and antibonding regions, which signifies a stable non-bonding state for the C2–F bond in the system.

3.2 Real-Time PFAS Degradation Dynamics on Electrified Electrode Surfaces

While the previous CEP ionic-relaxation calculations provide mechanistic information into the PFAS degradation process, they only give a single, time-independent snapshot of the degradation process near an equilibrium structure at zero Kelvin. To provide a time-dependent picture of the degradation dynamics, which also accounts for temperature effects, we carried out computationally-intensive CEP AIMD simulations of PFOA degradation on the Cu(111) surface. These AIMD simulations inherently explore a broader configurational and energetic landscape for the PFAS degradation process, whereas the CEP ionic-relaxation calculations are constrained to an initial geometry and can only explore configurations near the local energy minimum. Using the same PFOA/Cu(111) structure shown in Figs. S1(a) and (b) in the SI as an initial geometry, CEP AIMD calculations were carried out at -3.3 V for a duration of 1,307 fs. The SI provides a movie of the degradation dynamics of PFOA/Cu(111) and Figs. 3(a) and (b) show the final decomposed structure of PFOA obtained from our CEP AIMD calculations, The evolution of all 15 C−F bonds in PFOA during the CEP AIMD simulation is depicted in the inset of Fig. 3(c). At ∼1250 fs, the C5–F and C6–F bonds begin to stretch (by 35% and 73%, respectively) until they effectively dissociate, leading to the release of F atoms from the molecule and migration into the surrounding electrolyte solution. It is worth mentioning that we also carried out conventional AIMD calculations (which only allows a *fixed* number of electrons due to its closed-system nature) of PFOA on CU(111), and no bond dissociation of any kind was observed. In contrast, our CEP-based AIMD calculations clearly show the dissociation of C–F bonds in PFOA at -3.3 V, which demonstrates the new capability of the CEP approach for capturing electrochemically-induced bond-breaking processes.

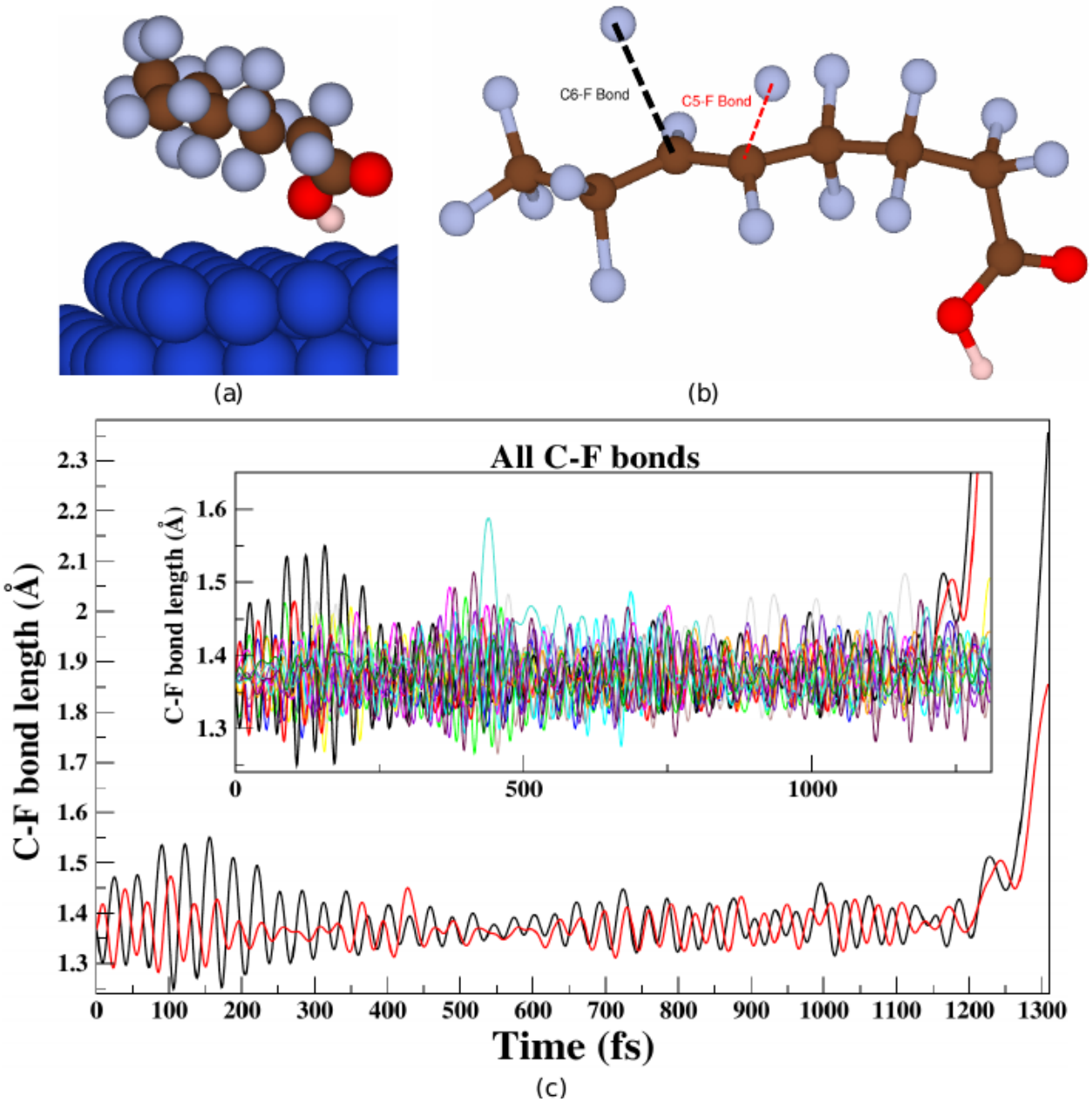

Figure 3: (a) Snapshot of the PFOA/Cu(111) supercell at the end (1,307 fs) of the CEP AIMD simulation at -3.3 V. (b) Magnified view of the PFOA molecule shown in panel (a). (c) Evolution of the C5–F (red) and C6–F (black) bonds, which dissociate during the CEP AIMD simulation. The atoms are denoted by the following coloring scheme: H (white), C (brown), O (red), F (gray), and Cu (blue).

Taken together, our quantum calculations corroborate several previous experimental and computational observations on PFAS degradation. For example, our CEP AIMD calculations at -3.3 V naturally predict the dissociation of the C5–F and C6–F bonds in PFOA, which were previously identified as having the lowest bond dissociation energies in a joint experimental/computational study (see Fig. 3(d) in Ref. 38). In addition, our ionic relaxation simulations predict that a C–F bond in PFOA dissociates at an applied external potential of -3.0 V, which aligns well with experimental findings.[33] Finally, our quantum calculations enable a Bader charge analysis to predict the distribution of electrons in PFAS, which provides insight into how charge is transferred to these contaminants in electrified environments to enable subsequent degradation reactions.

In conclusion, we have carried out the first constant-potential simulations of PFAS reactions on electrified surfaces to probe their degradation dynamics under realistic non-equilibrium conditions. These advanced CEP calculations provide new mechanistic details of PFAS degradation in an open system under an electrochemical bias, which cannot be gleaned from conventional DFT calculations. Specifically, our CEP calculations show that C–F anti-bonding states near the Fermi level (i.e., the chemical potential of the system) emerge when the system is placed under a negative bias. This subsequently causes the C–F bond to dissociate until the system reaches a stable non-bonding state where the bonding and anti-bonding states of PFAS are energetically separated. To provide time scales for this complex process, we also carried out large-scale CEP AIMD calculations of PFOA degradation on an electrified Cu(111) surface, which show that defluorination occurs within 1,307 fs when the system is placed under a negative bias of -3.3 V. Taken together, these CEP calculations enable a new capability for predicting reactions and time-resolved PFAS degradation mechanisms under realistic, non-equilibrium, electrochemical conditions. Specifically, our open-system quantum calculations enable predictions of chemical reactivity and elucidate the effect of external potentials on PFAS degradation on electrified surfaces. Moreover, these predictive CEP approaches hold immense promise for pre-screening candidate mate-

rial surfaces and predicting optimal electrochemical conditions/biases to guide experimental efforts in remediating PFAS and other emerging environmental contaminants. For example, our computational approach can facilitate the exploration of alternative electrode materials such as boron-doped diamond (BDD), lead oxide (PbO_2), and tin oxide (SnO_2) to provide mechanistic insight into PFOA oxidation and defluorination mechanisms on these different surfaces. Additionally, our approach can also be used to investigate the effect of electrolytes on PFAS degradation, which can further be used to improve treatment processes. Exploring all of these various aspects with our computational approaches can assist PFAS researchers in rationally down-selecting promising electrode materials and electrolytes to enhance the efficiency of experimental degradation strategies.

Funding Sources

This work was supported by the U.S. Department of Energy, Energy Efficiency & Renewable Energy (EERE) under Award No. DE-EE0010432.

Acknowledgement

This work used the Expanse supercomputer at the San Diego Supercomputer Center, through allocation TG-CHE240173 from the Advanced Cyberinfrastructure Coordination Ecosystem: Services & Support (ACCESS) program. Dr. Min Choi and Dr. Gabriel S. Phun are gratefully acknowledged for constructing the table of contents figure used in this work.

Supporting Information Available

CEP-movie of AIMD degradation dynamics of PFOA/Cu(111) at -3.3 V, figures of the optimized PFOA/Cu(111) supercell, and figures of optimized PFOA/Cu(111) supercells obtained from CEP ionic-relaxation calculations at several values of the applied bias.

References

(1) Schaider, L. A.; Balan, S. A.; Blum, A.; Andrews, D. Q.; Strynar, M. J.; Dickinson, M. E.; Lunderberg, D. M.; Lang, J. R.; Peaslee, G. F. Fluorinated Compounds in U.S. Fast Food Packaging. *Environmental Science & Technology Letters* **2017**, *4*, 105–111.

(2) Sajid, M.; Ilyas, M. PTFE-Coated Non-Stick Cookware and Toxicity Concerns: A Perspective. *Environmental Science and Pollution Research* **2017**, *24*, 23436–23440.

(3) Guelfo, J. L.; Adamson, D. T. Evaluation of a National Data Set for Insights into Sources, Composition, and Concentrations of Per- and Polyfluoroalkyl Substances (PFASs) in U.S. Drinking Water. *Environmental Pollution* **2018**, *236*, 505–513.

(4) Crone, B. C.; Speth, T. F.; Wahman, D. G.; Smith, S. J.; Abulikemu, G.; Kleiner, E. J.; Pressman, J. G. Occurrence of Per- and Polyfluoroalkyl Substances (PFAS) in Source Water and Their Treatment in Drinking Water. *Crit. Rev. Environ. Sci. Technol.* **2019**, *49*, 2359–2396.

(5) Su, Y.; Rao, U.; Khor, C. M.; Jensen, M. G.; Teesch, L. M.; Wong, B. M.; Cwiertny, D. M.; Jassby, D. Potential-Driven Electron Transfer Lowers the Dissociation Energy of the C–F Bond and Facilitates Reductive Defluorination of Perfluorooctane Sulfonate (PFOS). *ACS Applied Materials & Interfaces* **2019**, *11*, 33913–33922.

(6) Rao, U.; Su, Y.; Khor, C. M.; Jung, B.; Ma, S.; Cwiertny, D. M.; Wong, B. M.; Jassby, D. Structural Dependence of Reductive Defluorination of Linear PFAS Compounds in a UV/Electrochemical System. *Environmental Science & Technology* **2020**, *54*, 10668–10677.

(7) Yamijala, S. S. R. K. C.; Shinde, R.; Wong, B. M. Real-Time Degradation Dynamics of Hydrated Per- and Polyfluoroalkyl Substances (PFASs) in the Presence of Excess Electrons. *Phys. Chem. Chem. Phys.* **2020**, *22*, 6804–6808.

(8) Maza, W. A.; Breslin, V. M.; Owrutsky, J. C.; Pate, B. B.; Epshteyn, A. Nanosecond Transient Absorption of Hydrated Electrons and Reduction of Linear Perfluoroalkyl Acids and Sulfonates. *Environmental Science & Technology Letters* **2021**, *8*, 525–530.

(9) Biswas, S.; Yamijala, S. S. R. K. C.; Wong, B. M. Degradation of Per- and Polyfluoroalkyl Substances with Hydrated Electrons: A New Mechanism from First-Principles Calculations. *Environmental Science & Technology* **2022**, *56*, 8167–8175.

(10) Biswas, S.; Wong, B. M. Degradation of Perfluorooctanoic Acid on Aluminum Oxide Surfaces: New Mechanisms from Ab Initio Molecular Dynamics Simulations. *Environmental Science & Technology* **2023**, *57*, 6695–6702.

(11) Wang, Y.; Zhang, J.; Zhang, W.; Yao, J.; Liu, J.; He, H.; Gu, C.; Gao, G.; Jin, X. Electrostatic Field in Contact-Electro-Catalysis Driven C-F Bond Cleavage of Perfluoroalkyl Substances. *Angewandte Chemie International Edition* **2024**, *63*, e202402440.

(12) Román Santiago, A.; Baldaguez Medina, P.; Su, X. Electrochemical Remediation of Perfluoroalkyl Substances from Water. *Electrochimica Acta* **2022**, *403*, 139635.

(13) Su, Y.; Rao, U.; Khor, C. M.; Jensen, M. G.; Teesch, L. M.; Wong, B. M.; Cwiertny, D. M.; Jassby, D. Potential-Driven Electron Transfer Lowers the Dissociation Energy of the C–F Bond and Facilitates Reductive Defluorination of Perfluorooctane Sulfonate (PFOS). *ACS Applied Materials & Interfaces* **2019**, *11*, 33913–33922.

(14) Rao, U.; Su, Y.; Khor, C. M.; Jung, B.; Ma, S.; Cwiertny, D. M.; Wong, B. M.; Jassby, D. Structural Dependence of Reductive Defluorination of Linear PFAS Compounds in a UV/Electrochemical System. *Environmental Science & Technology* **2020**, *54*, 10668–10677.

(15) Biswas, S.; Wang, X.; Wong, B. M. Advanced Experimental and Computational Approaches for Advanced Reduction of Per- and Polyfluoroalkyl Substances. *Current Opinion in Chemical Engineering* **2024**, *44*, 101017.

(16) King, J. F.; Chaplin, B. P. Electrochemical Reduction of Per- and Polyfluorinated Alkyl Substances (PFAS): Is It Possible? Applying Experimental and Quantum Mechanical Insights from the Reductive Defluorination Literature. *Current Opinion in Chemical Engineering* **2024**, *44*, 101014.

(17) Biswas, S.; Wong, B. M. Beyond Conventional Density Functional Theory: Advanced Quantum Dynamical Methods for Understanding Degradation of Per- and Polyfluoroalkyl Substances. *ACS ES&T Engineering* **2024**, *4*, 96–104.

(18) Garza, A. J.; Bell, A. T.; Head-Gordon, M. Mechanism of CO_2 Reduction at Copper Surfaces: Pathways to C_2 Products. *ACS Catalysis* **2018**, *8*, 1490–1499.

(19) Zhao, X.; Liu, Y. Origin of Selective Production of Hydrogen Peroxide by Electrochemical Oxygen Reduction. *Journal of the American Chemical Society* **2021**, *143*, 9423–9428.

(20) Yu, S.; Levell, Z.; Jiang, Z.; Zhao, X.; Liu, Y. What is the Rate-Limiting Step of Oxygen Reduction Reaction on Fe–N–C Catalysts? *Journal of the American Chemical Society* **2023**, *145*, 25352–25356.

(21) Mathew, K.; Kolluru, V. S. C.; Mula, S.; Steinmann, S. N.; Hennig, R. G. Implicit Self-Consistent Electrolyte Model in Plane-Wave Density-Functional Theory. *J. Chem. Phys.* **2019**, *151*, 234101.

(22) Mathew, K.; Sundararaman, R.; Letchworth-Weaver, K.; Arias, T. A.; Hennig, R. G. Implicit Solvation Model for Density-Functional Study of Nanocrystal Surfaces and Reaction Pathways. *J. Chem. Phys.* **2014**, *140*, 084106.

(23) Hohenberg, P.; Kohn, W. Inhomogeneous Electron Gas. *Phys. Rev.* **1964**, *136*, B864–B871.

(24) Kohn, W.; Sham, L. J. Self-Consistent Equations Including Exchange and Correlation Effects. *Phys. Rev.* **1965**, *140*, A1133–A1138.

(25) Perdew, J. P.; Burke, K.; Ernzerhof, M. Generalized Gradient Approximation Made Simple. *Phys. Rev. Lett.* **1996**, *77*, 3865–3868.

(26) Xu, L.; Lin, J.; Bai, Y.; Mavrikakis, M. Atomic and Molecular Adsorption on Cu(111). *Topics in Catalysis* **2018**, *61*, 736–750.

(27) Jenness, G. R.; Shukla, M. K. What Can Blyholder Teach Us about PFAS Degradation on Metal Surfaces? *Environ. Sci.: Adv.* **2024**, *3*, 383–401.

(28) Bonnet, N.; Morishita, T.; Sugino, O.; Otani, M. First-Principles Molecular Dynamics at a Constant Electrode Potential. *Phys. Rev. Lett.* **2012**, *109*, 266101.

(29) Blöchl, P. E. Projector Augmented-Wave Method. *Phys. Rev. B* **1994**, *50*, 17953–17979.

(30) Kresse, G.; Joubert, D. From Ultrasoft Pseudopotentials to the Projector Augmented-Wave Method. *Phys. Rev. B* **1999**, *59*, 1758–1775.

(31) Grimme, S.; Antony, J.; Ehrlich, S.; Krieg, H. A Consistent and Accurate Ab Initio Parametrization of Density Functional Dispersion Correction (DFT-D) for the 94 Elements H-Pu. *Journal of Chemical Physics* **2010**, *132*, 154104.

(32) Evans, D. J.; Holian, B. L. The Nose–Hoover Thermostat. *Journal of Chemical Physics* **1985**, *83*, 4069–4074.

(33) Pud, A.; Shapoval, G.; Kukhar, V.; Mikulina, O.; Gervits, L. Electrochemical Reduction of Some Saturated and Unsaturated Perfluorocarbons. *Electrochimica Acta* **1995**, *40*, 1157–1164.

(34) Röckl, J. L.; Robertson, E. L.; Lundberg, H. Electrosynthetic C–F bond cleavage. *Org. Biomol. Chem.* **2022**, *20*, 6707–6720.

(35) Bader, R. *Atoms in Molecules: A Quantum Theory*; International Series of Monographs on Chemistry; Clarendon Press, 1990.

(36) Tang, W.; Sanville, E.; Henkelman, G. A Grid-Based Bader Analysis Algorithm without Lattice Bias. *Journal of Physics: Condensed Matter* **2009**, *21*, 084204.

(37) Nelson, R.; Ertural, C.; George, J.; Deringer, V. L.; Hautier, G.; Dronskowski, R. LOBSTER: Local Orbital Projections, Atomic Charges, and Chemical-Bonding Analysis from Projector-Augmented-Wave-Based Density-Functional Theory. *Journal of Computational Chemistry* **2020**, *41*, 1931–1940.

(38) Bentel, M. J.; Yu, Y.; Xu, L.; Li, Z.; Wong, B. M.; Men, Y.; Liu, J. Defluorination of Per- and Polyfluoroalkyl Substances (PFASs) with Hydrated Electrons: Structural Dependence and Implications to PFAS Remediation and Management. *Environmental Science & Technology* **2019**, *53*, 3718–3728.

TOC Graphic